Electronic Supplementary Material (ESI) for Journal of Materials Chemistry B.

Supplementary information

Metastable $FeSe_2$ nanosheets as a one-for-all platform for stepwise synergistic tumor therapy

Naiyue Zhang,[a,1] Liwen Jiang,[b,1] Yumeng Yue,[a] Xiaomin Zhao,[b] Yanwei Hu,[a] Yali Shi,[a] Liying Zhao,[b] Dawei Deng.*[ab]

[a] *Department of Biomedical Engineering, and* [b] *Department of Pharmaceutical Engineering, School of Engineering, China Pharmaceutical University, Nanjing 211198, China.*

[1] Naiyue Zhang and Liwen Jiang contributed equally to this work.

* *Corresponding Author*

E-mail: dengdawei@cpu.edu.cn (D. Deng)

Materials

Selenium powder (Se, 99.9%), anhydrous sodium sulfite (Na_2SO_3, 98%), ethylene glycol (EG, 99%), Iron (II) chloride tetrahydrate ($FeCl_2 \cdot 4H_2O$, 99.95%), mercaptoacetic acid (TGA, 95%), glutathione (GSH, 98%), Rhodamine B (RB, 97%), anhydrous ethanol and other chemical reagents were purchased from Maclean's Biochemical Technology. 3,3',5,5'-tetramethyl Benzidine (TMB, 98%), 5,5'-dithiobis (2-nitrobenzoic acid) (DTNB, 98%), 3-(4,5-dimethyl-2-thiazolyl)-2,5-diphenyltetrazole bromide (MTT) and Dimethyl sulfoxide (DMSO, 99.9%) were purchased from Shanghai Aladdin Biotechnology Co., Ltd. RPMI-1640 medium, Fetal bovine serum (FBS), phosphate buffer solution (PBS), trypsin-EDTA Solution, 4% paraformaldehyde fix solution, reactive oxygen species assay kit, DAPI staining solution, lipid peroxidation sensor (C11-BODIPY$^{581/591}$), reactive oxygen species fluorescent probe (ROS Brite 700), mouse breast cancer cells (4T1) and human normal breast epithelial cells (MCF 10A) were purchased from KeyGEN Biotechnology Co., Ltd. Calcein/PI cell viability/cytotoxicity assay kit, Annexin V-FITC apoptosis detection kit, GSH and GSSG assay kit, Amplex red, Mito-Tracker Green, cellular glutathione peroxidase assay kit and mitochondrial membrane potential assay kit were purchased from Shanghai Beyotime Biotechnology Co., Ltd.

Characterization

TEM images were taken by an HT7700 transmission electron microscopy (Hitachi, Japan). HRTEM images were taken by a Tecnai G2 F30 high-resolution transmission electron microscopy (FEI, USA). The AFM image was taken by atomic force microscopy (Bruker, Germany). XRD was obtained by D8 ADVANCE X-ray powder diffractometer (Bruker, Germany). XPS was measured using the ESCALAB 250Xi X-ray photoelectron spectrometer (Thermo Fisher, USA). UV-vis-NIR absorption spectrum was measured using the UV-2600 spectrophotometer (Shimadzu, Japan). Fluorescence spectrum was determined via Shanghai Prism UV Fluorescence Spectrophotometer. EPR spectrum was measured using the EMX 10/12 electron paramagnetic resonance spectrometer (Bruker, Germany). Cell uptake analysis was

carried out by a dark field microscopy (CYTOVIVA, USA). Cell viability was measured by a microplate reader (Bethen Instruments, USA), Cell fluorescence images were measured by an inverted fluorescence microscope (Olympus, Japan) or a confocal laser scanning microscope (CLSM, Olympus, Japan). The flow cytometry was carried out using a flow cytometer (BD, USA). The biodistribution in vivo was determined by inductively coupled plasma atomic emission spectrometry (ICP-OES, Thermo Fisher Scientific, USA). In vivo fluorescence was detected by a small animal imaging system (IVIS, PerkinElmer Instrument Co., Ltd.).

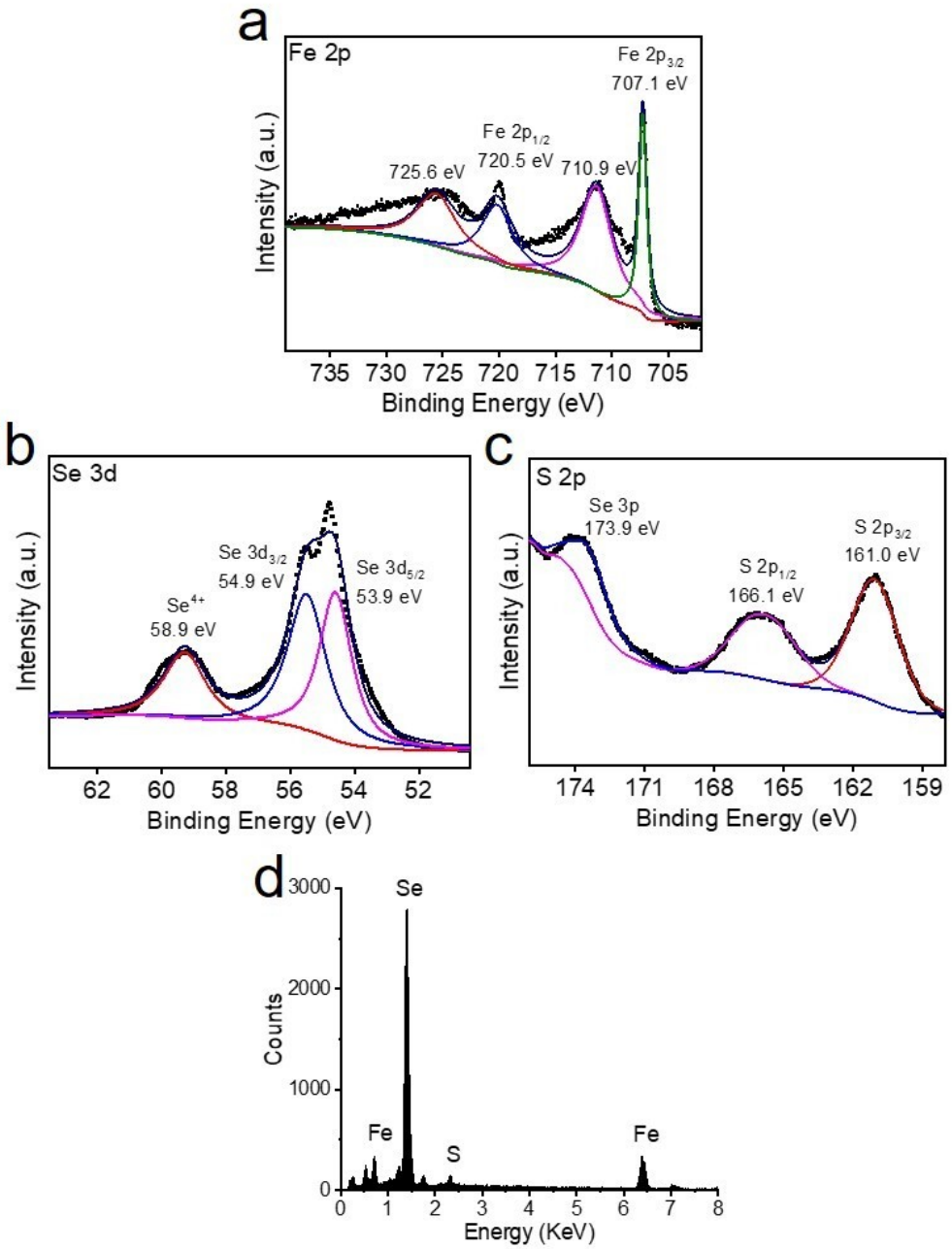

Fig. S1. (a-c) Fe 2p, Se 3d and S 2p XPS spectra of $FeSe_2$ NSs. These XPS spectra were obtained from a sample power of $FeSe_2$. (d) the EDX spectrum of $FeSe_2$ NSs formed from the self-assembly of NPs.

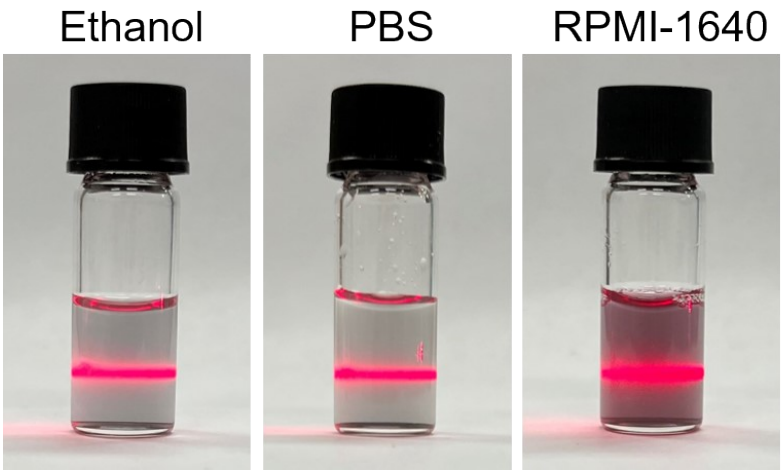

Fig. S2. Photographs of the $FeSe_2$ NSs dispersed in different solutions. The excellent water dispersion of the $FeSe_2$ NSs was confirmed by the Tindahl effect with laser irradiation.

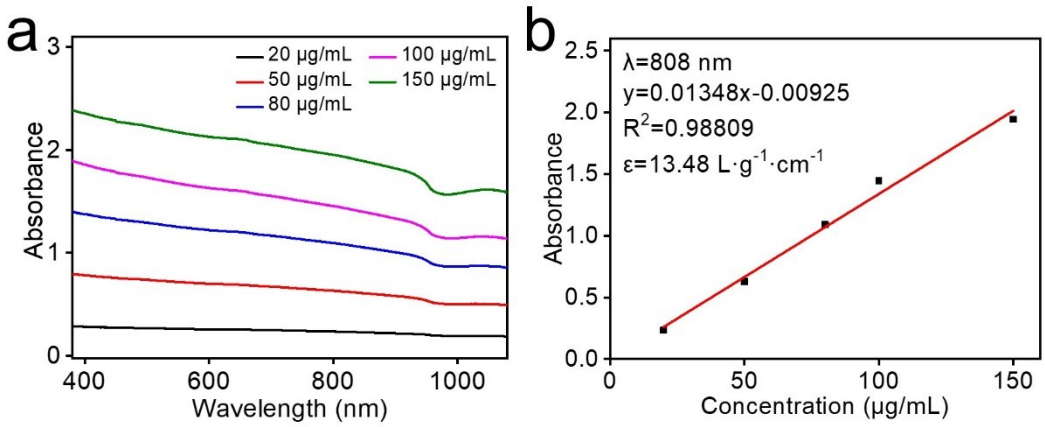

Fig. S3. (a) UV-vis absorption spectra of $FeSe_2$ NSs with different concentrations. (b) Mass extinction coefficient of $FeSe_2$ at 808 nm.

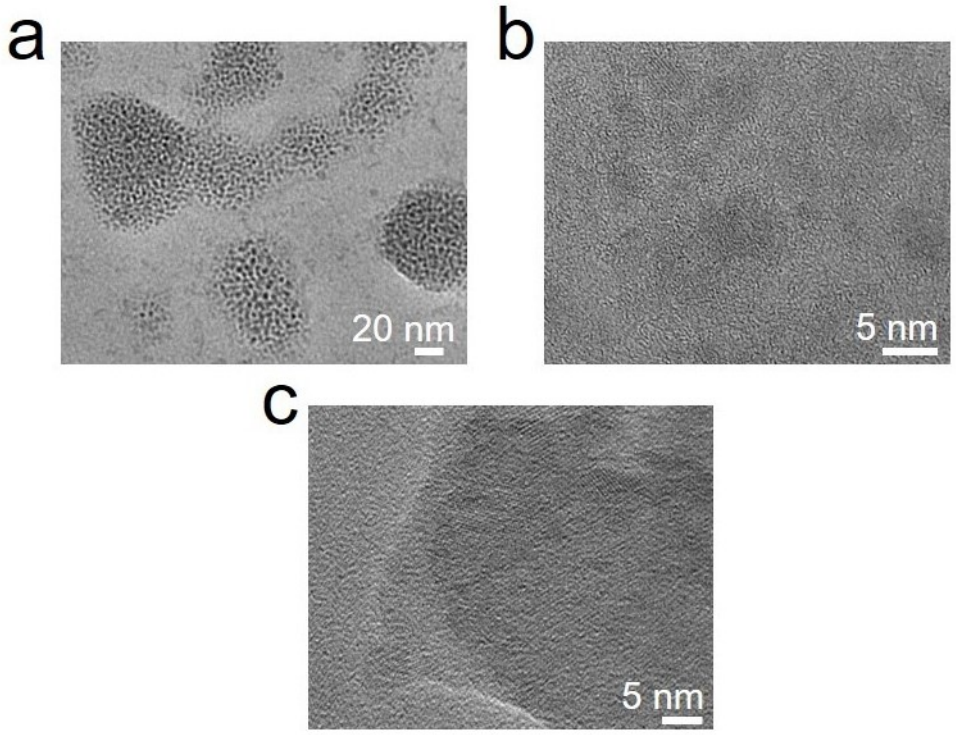

Fig. S4. (a, b) HR-TEM images of $FeSe_2$ nanoparticles reaction for 1 min after injection of selenium source. (c) HR-TEM image of $FeSe_2$ NSs formed at about 15 min.

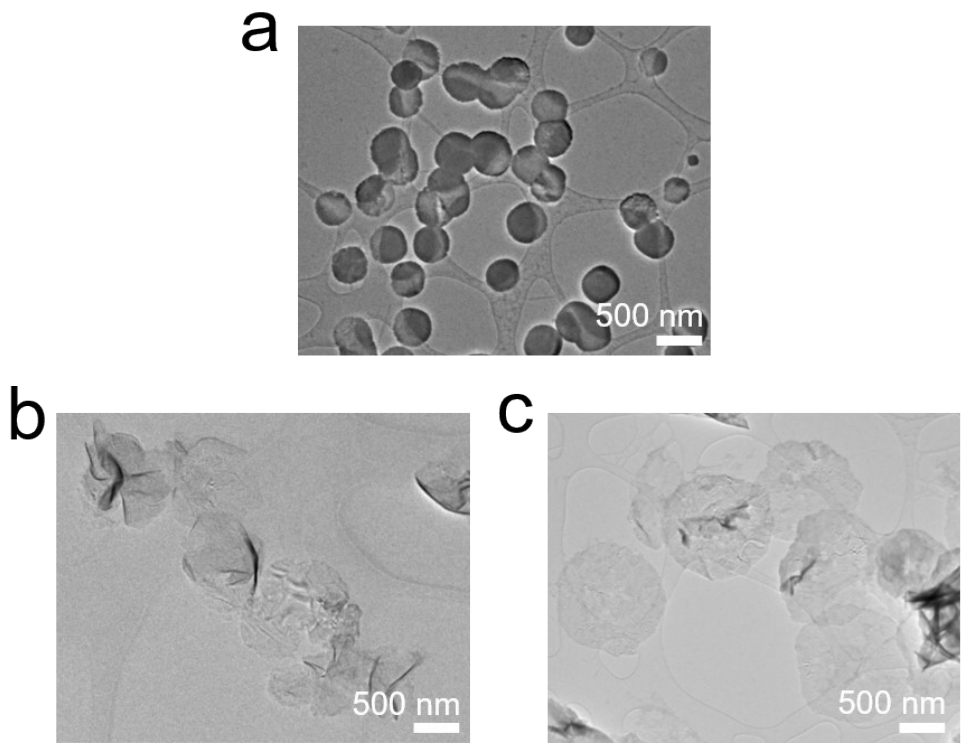

Fig. S5. TEM images of $FeSe_2$ NSs with increased diameters: (a) 400 nm, (b) 700 nm and (c) 1200 nm. Scale bar = 500 nm.

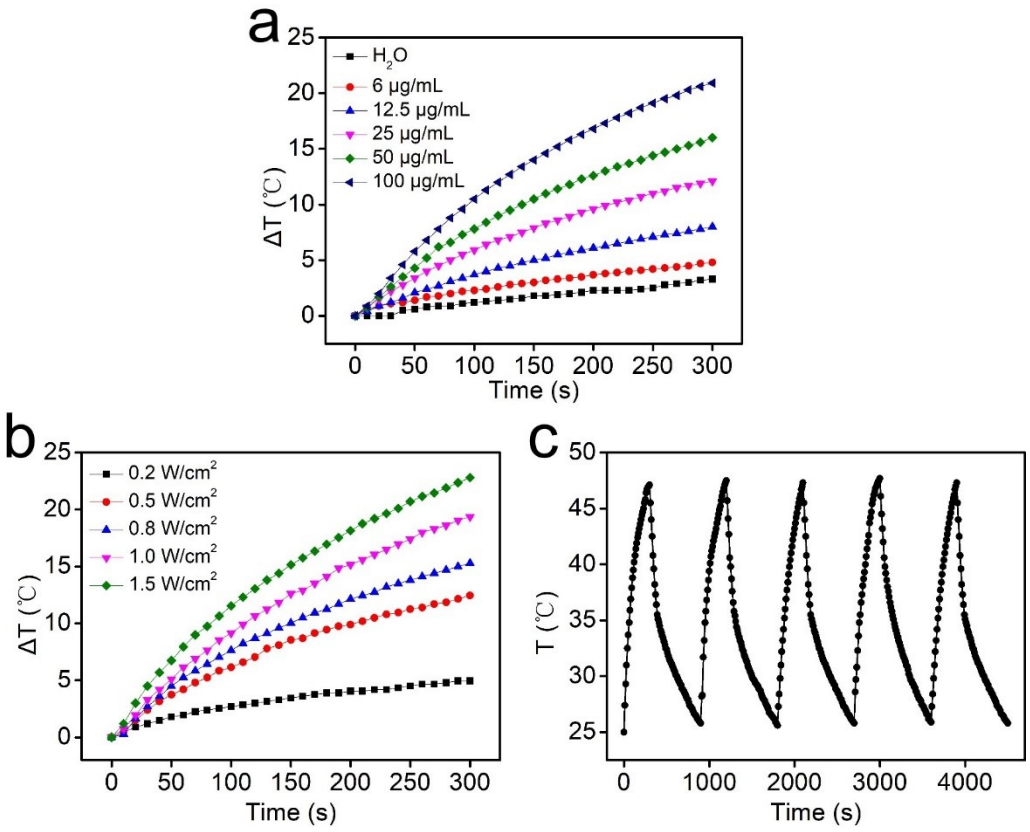

Fig. S6. (a) Temperature variations of $FeSe_2$ NSs solutions with different concentrations under the irradiation for 5 min (808 nm, 1 W/cm^2). (b) Temperature variations of $FeSe_2$ NSs solutions (100 μg/mL) under the 808 nm irradiation for 5 min at different laser power densities. (c) Temperature variations during five heating-cooling cycles.

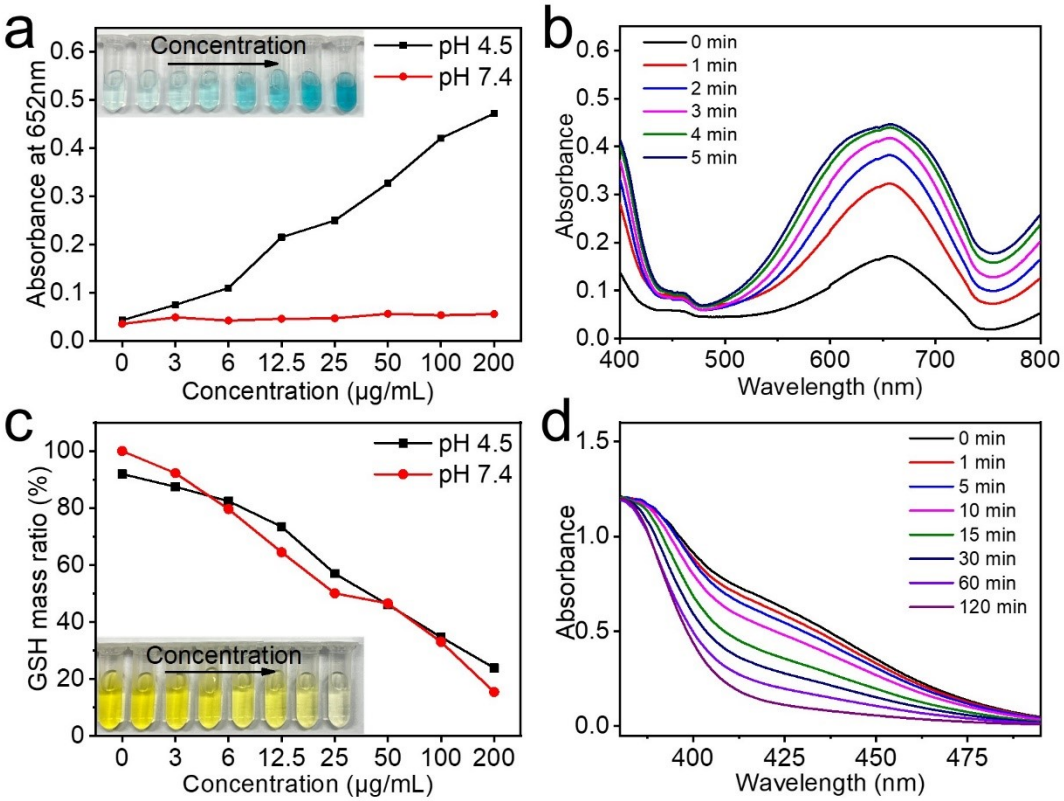

Fig. S7. (a) Changes in the absorbance values (at 652 nm) of TMB solutions containing increased FeSe2 concentration at pH 4.5 or at pH 7.4. (b) UV-vis absorption spectra of the POD-like activities of FeSe2 NSs over time by TMB method. (c) Changes in the absorbance values (at 412 nm) of DTNB solutions containing increased FeSe2 concentration at pH 4.5 or at pH 7.4. (d) UV-vis absorption spectra of the GSHOx-like activities of FeSe2 NSs over time by DTNB method.

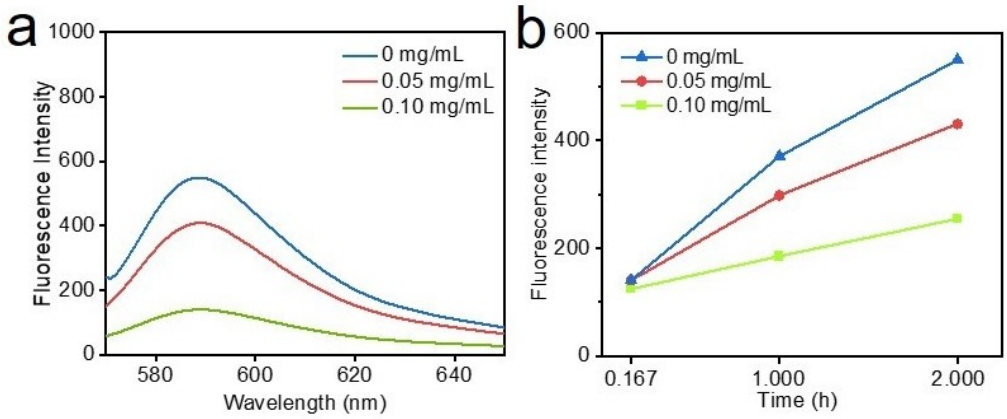

Fig. S8. (a) Generation of H_2O_2 after incubation with $FeSe_2$ NSs for 2 h was determined in 585 nm. (b) The generation of H_2O_2 in GSH solution after treated with $FeSe_2$ NSs for different time.

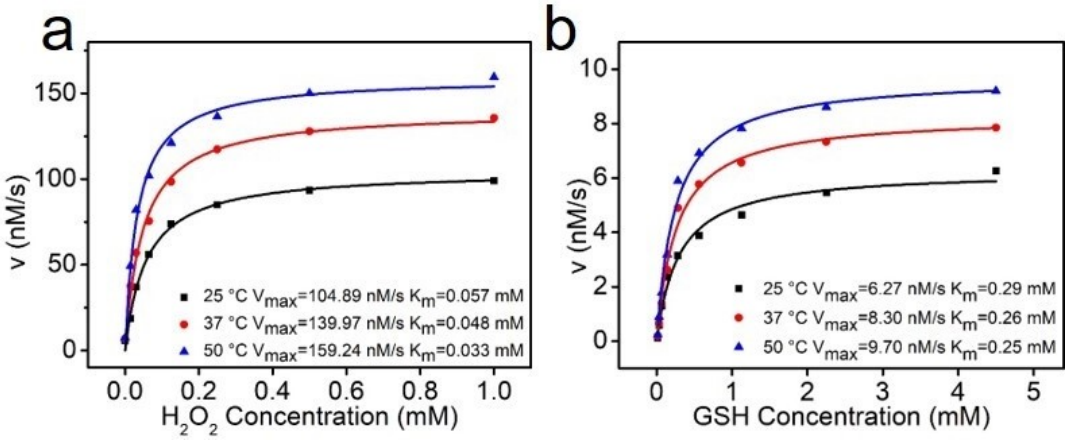

Fig. S9. Kinetic assay of POD-like (a) and GSHOx-like (b) activities using H_2O_2 and GSH as substrates, respectively.

Table S1. V_{max} and K_m values of various nanozymes.

	POD-like	GSHOx-like	ref

	V_{max} (nM/s)	K_m (mM)	V_{max} (nM/s)	K_m (mM)	
Fe_3O_4	104.4	135.3			[1]
FeS_2	135.4	0.041	980	0.66	[2]
Co-$FeSe_2$	27.5	2.74			[3]
$FeSe_2$	159.24	0.033	9.7	0.25	This work

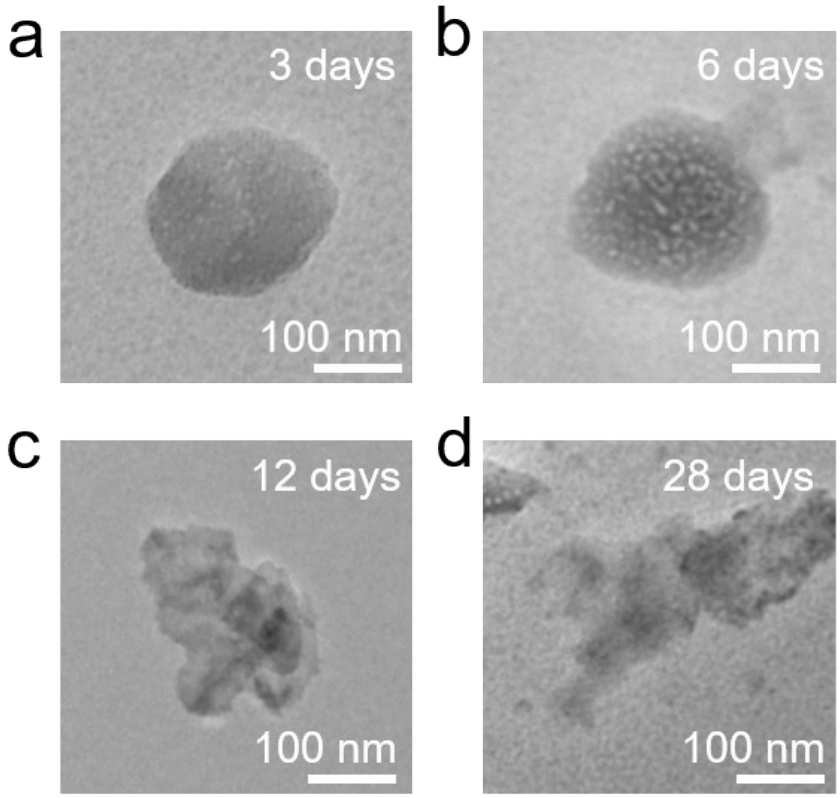

Fig. S10. TEM images of $FeSe_2$ NS prepared at the TGA/Fe ratio of 4/1 and stored in PBS for different days, showing $FeSe_2$ NS stored in PBS can maintain the stability for almost one month. Scale bar = 100 nm.

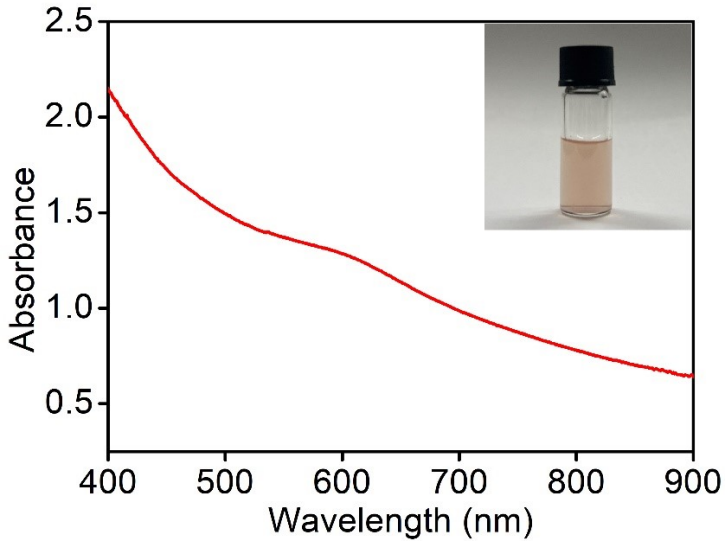

Fig. S11. UV-vis absorption spectra of the non-stationary state of red selenide generated at the TGA/Fe ratio of 1/1[4].

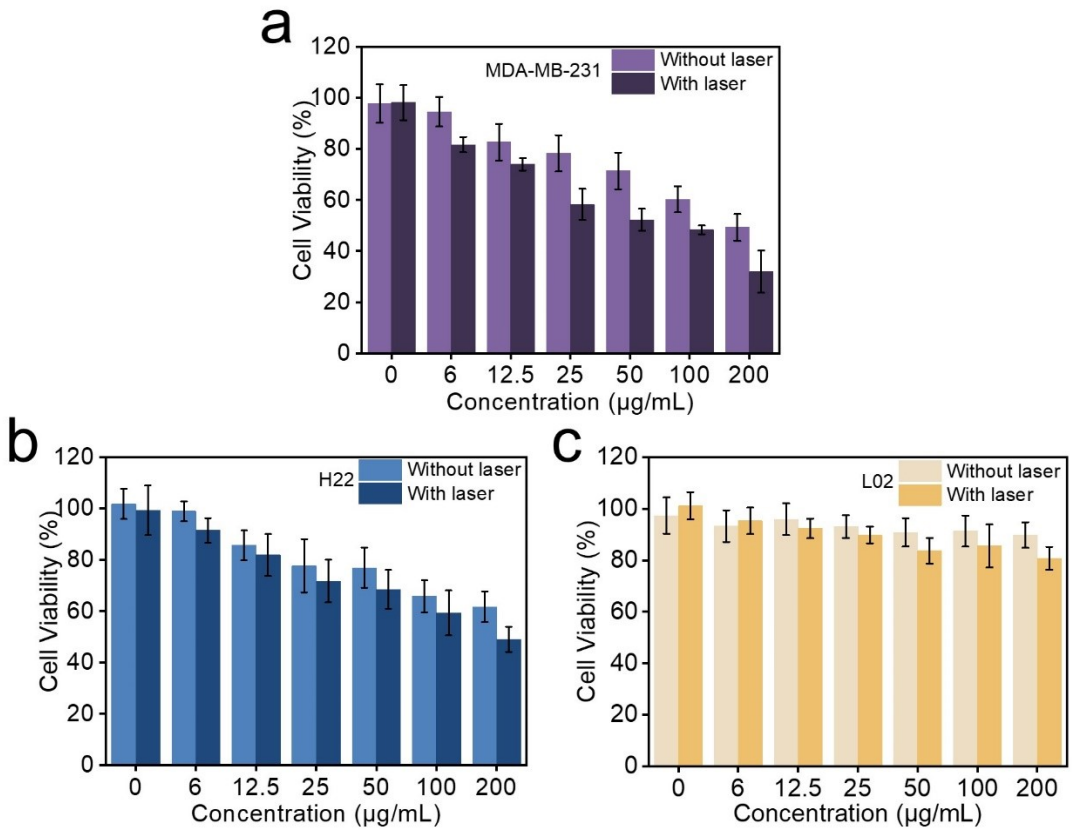

Fig. S12. Cell viabilities during on/off the laser irradiation (808 nm, 1.0 W/cm^2) of (a) MDA-MB-231, (b) H22 and (c) L02 cells incubated with $FeSe_2$ NSs (n=5).

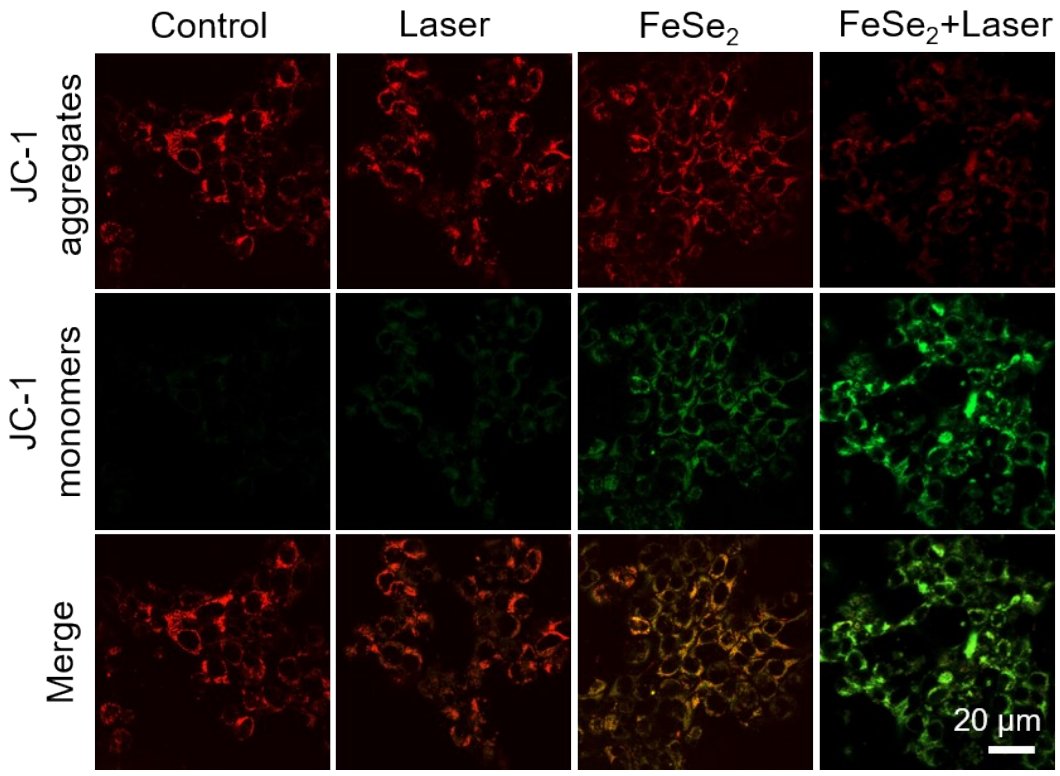

Fig. S13. Changes of mitochondrial membrane potential in 4T1 cells after different treatments. Red JC-1 aggregate indicates mitochondria with a normal membrane potential, and the green JC-1 monomer means the mitochondria with a depolarized membrane (impaired mitochondria). Scale bar = 20 μm.

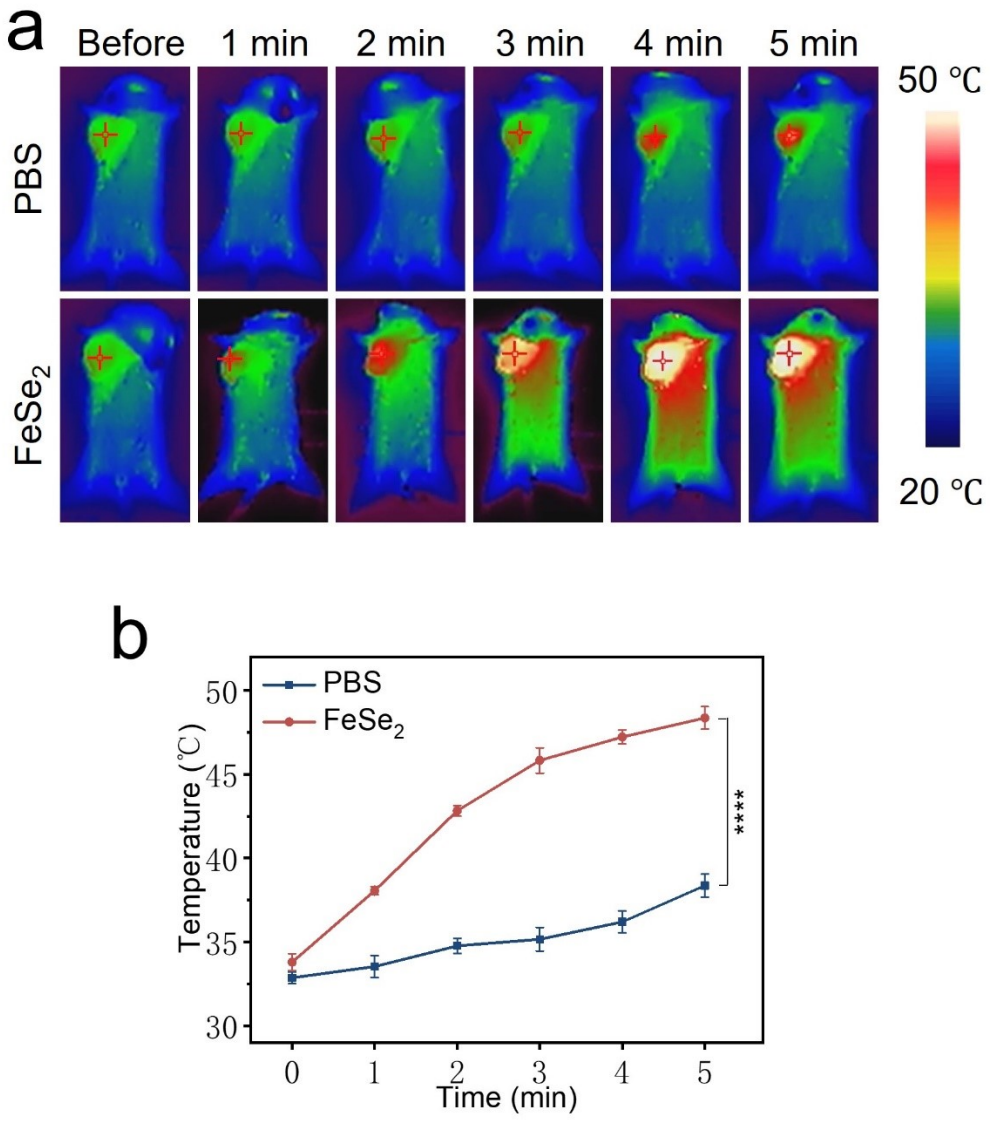

Fig. S14. (a) Infrared thermal imaging images of mice irradiated with laser (808 nm, 1 W/cm^2) at different times on tumor sites 6 h after injection of PBS or $FeSe_2$ NSs, and (b) the corresponding temperature values acquired within 5 min.

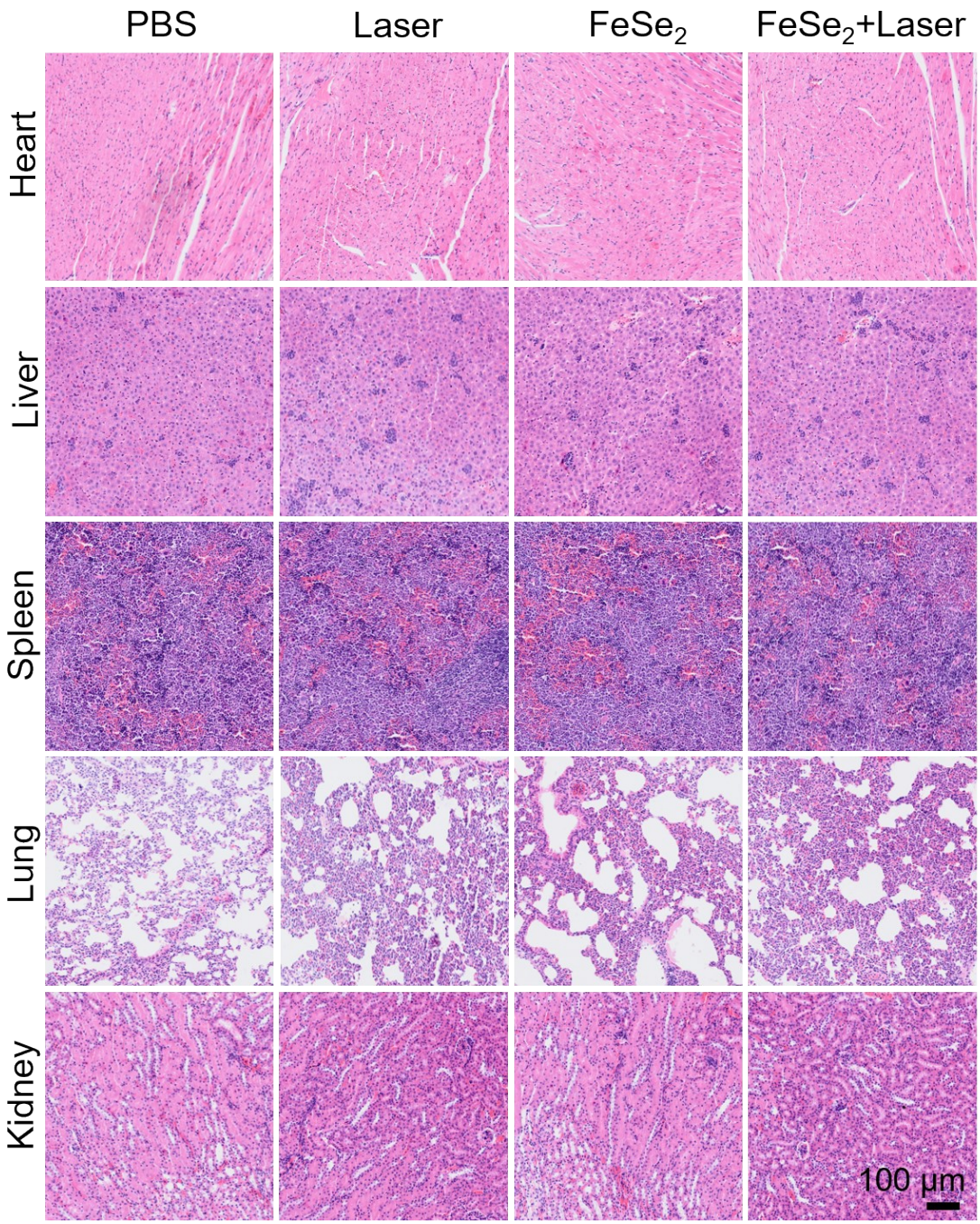

Fig. S15. H&E staining images of major organs in 4T1 breast tumor-bearing mice. Scale bar = 100 μm.

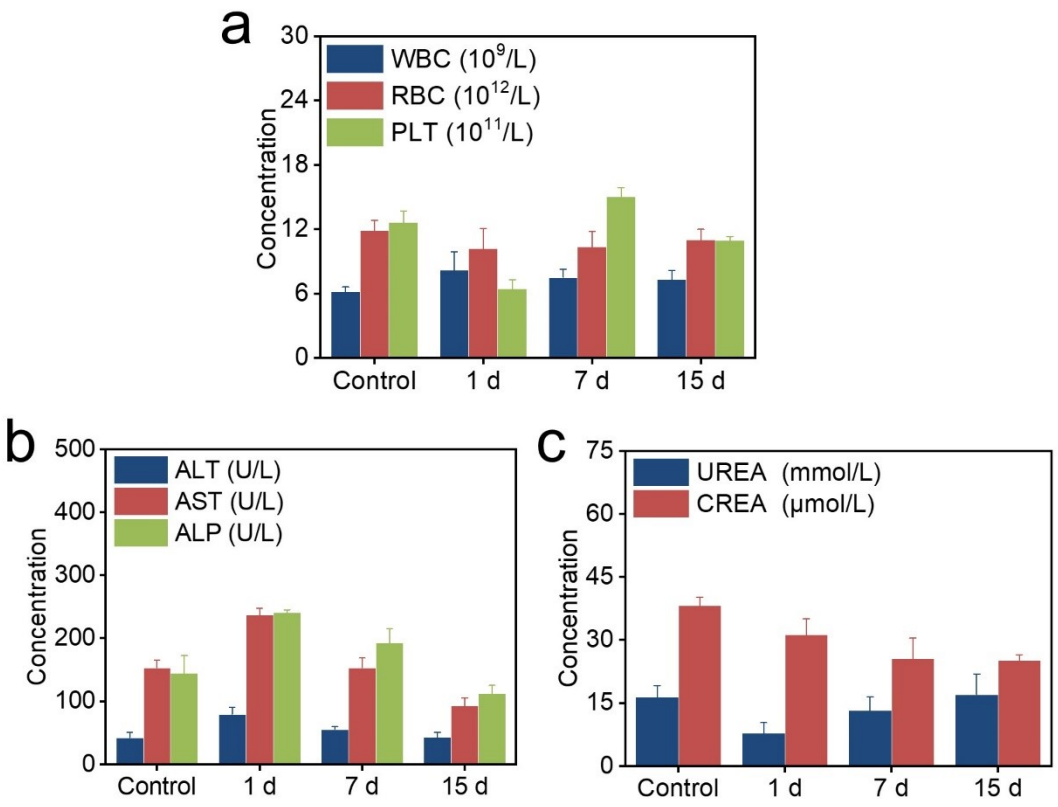

Fig. S16. (a) The blood routine indicators and serum biochemical analysis including (b) liver function and (c) renal function results of mice at different time points after the therapy(n=3).

References

1. L. Gao, J. Zhuang, L. Nie, J. Zhang, Y. Zhang, N. Gu, T. Wang, J. Feng, D. Yang, S. Perrett and X. Yan, *Nat. Nanotechnol*, 2007, **2**, 577-583.
2. X. Meng, D. Li, L. Chen, H. He, Q. Wang, C. Hong, J. He, X. Gao, Y. Yang, B. Jiang, G. Nie, X. Yan, L. Gao and K. Fan, *ACS Nano*, 2021, **15**, 5735-5751.
3. J. Zhang, E. Ha, D. Li, S. He, L. Wang, S. Kuang and J. Hu, *J. Mat. Chem. B*, 2023, **11**, 4274-4286.
4. S. Dhanjal and S. S. Cameotra, *Microb. Cell. Fact.*, 2010, **9**, 52.